CenterlinePointNet++: A New Point Cloud Based Architecture for Coronary Artery Pressure Drop and vFFR Estimation

Patryk Rygiel[1], Paweł Płuszka[1], Maciej Zięba[2], and Tomasz Konopczyński[1(✉)]

[1] Hemolens Diagnostics Sp. z o.o., Wrocław, Poland
{patryk.rygiel,pawel.pluszka,tomasz.konopczynski}@hemolens.eu
[2] Wroclaw University of Science and Technology, Wrocław, Poland

Abstract. Estimation of patient-specific hemodynamic features, and in particular fractional flow reserve (FFR) in coronary arteries is an essential step in providing personalized and accurate diagnosis of coronary artery disease (CAD). In recent years, in the domain of computed tomography angiography (CTA), a virtual FFR (vFFR) derived from coronary CTA using computational fluid dynamics (CFD), has been used as a compelling, non-invasive, *in-silico* replacement for invasive diagnostic techniques. Unfortunately, the time and computational demands of CFD are major obstacles to introducing vFFR from CT as a commonly used prophylactic tool. In this work, we propose a novel geometric-based artificial deep learning (DL) architecture, CenterlinePointNet++, which acts as a surrogate for CFD engines for the task of hemodynamic features estimation of the coronary arteries. Our architecture works directly on the vessel geometry represented as a surface point cloud and a centerline graph. As a result of that, it utilizes implicit geometry embedding without the need for hand-crafted features to estimate directly hemodynamic features. We evaluate our approach on the task of pressure drops and vFFR estimation for a synthetically generated dataset of coronary arteries and showcase significant improvement over commonly used geometry-based approaches.

Keywords: deep learning · geometric deep learning · point clouds · CAD · FFR · hemodynamics

1 Introduction

Estimation of patient-specific hemodynamic features in coronary arteries is an essential step in providing personalized and accurate diagnosis and treatment of CAD which is one of the main causes of death in the world [15]. In the assessment of CAD, one of the most important biomarkers is a Fractional Flow Reserve

Supplementary Information The online version contains supplementary material available at https://doi.org/10.1007/978-3-031-43990-2_73.

H. Greenspan et al. (Eds.): MICCAI 2023, LNCS 14226, pp. 781–790, 2023.
https://doi.org/10.1007/978-3-031-43990-2_73

(FFR [3]), measured during an invasive coronary angiography procedure. With developments in CT and CFD, non-invasive approaches for accurate hemodynamic features estimation such as vFFR in patients with suspected ischemic heart disease became possible [9]. Unfortunately, although CFD offers a compelling *in-silico* replacement for invasive coronagraphy procedures, prolonged vFFR computation times, over many hours, have been a major concern [14].

To solve the computation time drawback, AI-based solutions have been proposed to lower the estimation time of vFFR down to minutes, or even seconds at the cost of accuracy [1,22]. Itu et al. [8] propose to compute a set of local and global hand-crafted features from the coronary anatomy to create a representation of a local stenotic segment. Based on this representation, a multilayer perceptron (MLP) model is trained to perform an FFR regression in the stenotic areas. They experiment on a dataset of 12,000 synthetically generated coronary geometries and evaluated the model on 125 patient-specific anatomical models extracted from CTA, reporting a correlation of 0.729 with invasive FFR on real anatomical models. Wang et al. [24] propose a similar method that utilizes hand-crafted features to feed a recurrent neural network (RNN) to estimate the FFR along the coronary artery. Authors experiment with training on 71 patient-specific anatomies extracted from CTA and report a correlation of 0.686 with invasive FFR measurement. Both approaches report compiling results of the vFFR estimation and showcase a drastic improvement in time consumption: 2.4 s for Itu et al. [8] and 120 s for Wang et al. [24]. The main drawback in both cases is the utilization of hand-crafted features. Additionally, authors do not share details of their features making their work impossible to reproduce [20]. A natural improvement over these methods would be an implicit feature learning method that could be performed on a vessel surface modelled as a mesh or a point cloud. However, there is no such method known to the authors that would tackle the problem of vFFR estimation for coronary arteries from CTA. For a similar task, Li et al. [11] propose a PointNet-like [17] architecture to predict velocity and pressure fields on point cloud geometries containing aorta, coronary arteries and bypass graft. Similarly, Suk et al. [21] utilizes mesh-based neural networks [5,6,23] to estimate wall shear stress along the vessels. Both approaches would be unsuitable for the vFFR estimation from CTA, as it would require the processing of more complex, elongated geometries.

In this work, we tackle the problem of estimating hemodynamic features such as pressure drops and vFFR along the coronary arteries extracted from CTA. We propose a novel CenterlinePointNet++ architecture that is tailored towards the processing of complex, elongated structures such as coronary arteries, that can be represented as a surface point cloud and a centerline graph along branches. In our approach, implicit feature extraction is guided by the proposed centerline grouping aggregation. It is a replacement for the commonly used topology-agnostic [18], centerline-agnostic [7,19] or connectivity-based [25] aggregation strategies. To our best knowledge, this is the first method that is tackling the problem of pressure drops and vFFR estimation utilizing a point cloud neural network. We train and evaluate our approach on different scenarios

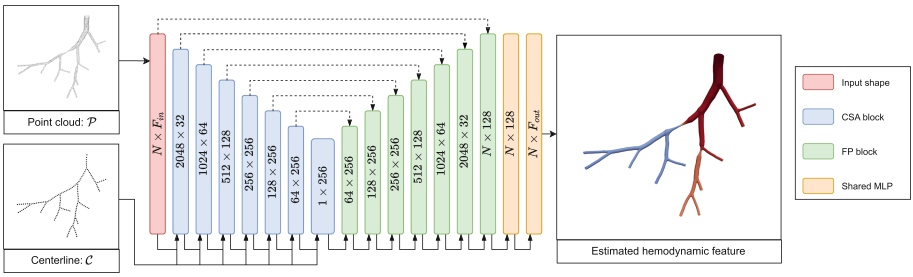

Fig. 1. Diagram of CenterlinePointNet++ architecture. The model incorporates an encoder-decoder structure seen in PointNet++. The encoder branch consists of seven CSA blocks that process the surface point cloud and centerline graph. The decoder branch is built out of seven FP blocks and topped with the head consisting of two Shared MLP layers.

on the dataset of 1,700 synthetically generated coronary arteries. We test the model capability for two tasks: estimation of pressure drop and vFFR under different GT CFD settings. For each setting, we report an improvement over Euclidean distance based grouping in terms of Mean Absolute Error (MAE) and Normalized Absolute Error (NMAE). We further test the approach performance of vFFR estimation and report a correlation with CFD vFFR of 0.93.

2 Method

In this section, we provide a detailed description of the proposed CenterlinePointNet++ architecture (see Fig. 1) for the problem of estimating hemodynamic features. We improve upon the well-known PointNet++ architecture [18] by taking into account *a priori* knowledge of coronary arteries geometries. We extend its input to accept an additional channel with a centerline graph and change its encoder blocks to the proposed Centerline-Set-Abstraction (CSA) blocks that utilize the centerline graph and the centerline grouping method which facilitates geodesic metric. We refer to the input vessel mesh as $\mathcal{M}$ and the point cloud representing its surface that is sampled by extracting all its vertices is denoted as $\mathcal{P}$. The centerline graph, which can be extracted from the mesh with an algorithm of choice is denoted as $\mathcal{C} = (V_\mathcal{C}, E_\mathcal{C})$, where $V_\mathcal{C}$ is the set of nodes and $E_\mathcal{C}$ a set of undirected edges. Since the centerline graph is a 3D structure in Euclidean space, we can represent each $v \in V_\mathcal{C}$ as a point with 3D coordinates. The architecture takes as an input a point cloud $\mathcal{P}$ and centerline graph $\mathcal{C}$ and returns per-point hemodynamic features of choice. The details of the method are described in the following sections.

2.1 Encoder

The encoder is built out of the proposed CSA blocks in a hierarchical manner as it is shown in Fig. 1. It consists of n number of CSA blocks down to the

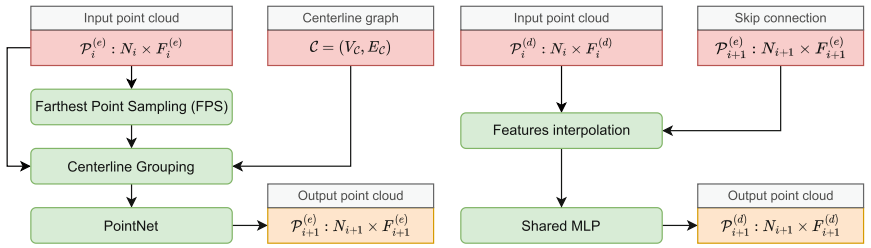

(a) CSA block (b) FP block

Fig. 2. CenterlinePointNet++ blocks. The CSA block performs feature extraction by downsampling point cloud with the FPS algorithm, aggregating surface points in a centerline-guided manner and processing them with PointNet. The FP block performs the upsampling procedure by interpolating features onto the new points passed via skip-connection and processing them with the Shared MLP layer.

bottleneck. Each CSA_{i+1} takes as an input a point cloud $\mathcal{P}_i^{(e)}$ of dimensions $N_i \times F_i^{(e)}$ from the previous block and a centerline graph $\mathcal{C}$, where N stands for the number of points, F stands for the number of features, $i+1$ is the index of the current CSA block, i is the index of the previous block, and (e) stands for "encoding". The CSA block is described in Fig. 2a. In the first step of a CSA block, a representative sampling procedure in form of Farthest Point Sampling [4] (FPS) is utilized to downsample $\mathcal{P}_i^{(e)}$ and create a representative point cloud $\mathcal{R} \subseteq \mathcal{P}$.

For each point $r \in \mathcal{R}$, a *centerline grouping* procedure $g(r, \mathcal{C})$ is performed to extract their point neighborhoods $\mathcal{G}_r \subseteq \mathcal{P}$. In the last step, all extracted neighbourhoods are processed independently with a PointNet [17] to construct neighbourhood feature vectors for all the points in $\mathcal{R}$.

Centerline Grouping: We propose a novel centerline-guided point grouping scheme for point cloud structures. Commonly used Euclidean distance based grouping strategies do not take into account an underlying surface manifold formed by the points. Thus they tend to fail when the point cloud topology is complex, by considering points in the close Euclidean distance to be neighbours while their distance along the formed manifold is much larger (see Fig. 3a). By utilizing a centerline-guided point grouping, the geodesic metric is facilitated, and thus the point neighbourhoods are constructed along the manifold (see Fig. 3b). Additionally, grouping along the centerline allows for a robust sequential embedding of the complex vessel trees and thus facilitates the learning of hemodynamic features.

For a given point cloud $\mathcal{P}$, its representation $\mathcal{R}$ and its centerline $\mathcal{C}$, the centerline grouping procedure $g(r, \mathcal{C})$ is performed independently for each $r \in \mathcal{R}$. We define a mapping function $M : \mathcal{P} \mapsto V_\mathcal{C}$, which assigns a closest, in Euclidean distance sense, centerline node $v \in V_\mathcal{C}$ to each point $p \in \mathcal{P}$. Since a

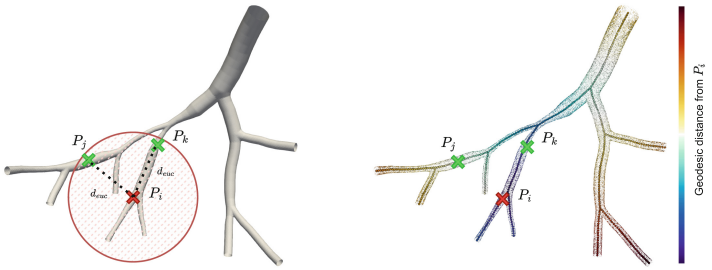

(a) Euclidean grouping. (b) Centerline grouping.

Fig. 3. Grouping comparison. Points P_j and P_k are considered to be in the same size neighborhood of P_i when grouped with Euclidean distance, even though their geodesic distances are substantially different. Grouping along the centerline solves this issue by facilitating geodesic metric.

representative point cloud $\mathcal{R}$ is a subset of point cloud $\mathcal{P}$, the mapping is also defined for each point $r \in \mathcal{R}$. Due to the utilization of a mapping function M, the grouping procedure can be performed directly on the centerline graph $\mathcal{C}$ where the topological structure of the vessel tree can be more accurately represented. Based on the 3D coordinates of centerline nodes $V_\mathcal{C}$, the weights of the edges $E_\mathcal{C}$ are calculated as distances between the connected nodes - since the centerline graph is not-mutable during training, the weights can be pre-computed in the pre-processing stage.

Having a mapping function M we can directly work on the centerline graph itself and thus we define a centerline neighbourhood $\mathcal{Q}_v$ which is computed independently for each $v \in M[\mathcal{R}]$ and can be expressed with the following equation:

$$\mathcal{Q}_{v_0} = \{v \in V_c : d_\mathcal{C}(v, v_0) \leq t\}, \tag{1}$$

where $d_\mathcal{C}$ is a centerline distance function which returns the length of the weighted shortest path between two given nodes in the centerline $\mathcal{C}$ and t is the distance threshold which marks whether nodes should be considered neighbours or not. Having centerline neighbourhoods Q extracted we need to map them back onto the point cloud $\mathcal{P}$ to obtain the point neighbourhoods $\mathcal{G}$ for each $r \in \mathcal{R}$:

$$\mathcal{G}_r = \{p \in P : M(p) \in \mathcal{Q}_{M(r)}\}. \tag{2}$$

2.2 Decoder

The decoder is built out of the Feature-Propagation (FP) blocks in a similar manner as in PointNet++ [18]. Its architecture is shown in Fig. 2b The FP takes as an input a point cloud $\mathcal{P}_i^{(d)}$ from the previous block and a reference point cloud $\mathcal{P}_{i+1}^{(e)}$ passed via skip-connection from the respective encoder block, where

$i+1$ is the index of the current FP block, i is the index of the previous block and (d) stands for "decoding". In the first step, the features from the point cloud $\mathcal{P}_i^{(d)}$ are interpolated onto the $\mathcal{P}_{i+1}^{(e)}$ by averaging features of three nearest neighbours in Euclidean distance sense. The resulting point cloud $\mathcal{P}_{i+1}^{(d)}$ is then processed with shared MLP which is applied independently to each $p \in \mathcal{P}_{i+1}^{(d)}$ to form new per-point feature vectors.

3 Experiments

In this section, we describe our evaluation of the proposed model architecture in the tasks of pressure drops and vFFR estimation of a synthetic coronary artery geometry with respect to different stenosis severity grades and different biologically relevant ranges of blood flow characteristics. We test our architecture against standard PointNet++ grouping with the same number of adequate layers as a reference due to the impossibility of reproduction [20] of the other two known relevant methods [8,24]. We train CenterlinePointNet++ and PointNet++ with the same set of hyperparameters. Both need approximately 15 s for inference on the RTX 3090 24 GB graphic card. The models are trained for 500 epochs with the batch size of 8 and `Adam` optimizer with the default constant learning rate of 0.001. For the loss function we use the Mean Squared Error (MSE) which is the mean of per point squared errors.

3.1 Dataset

We utilize a dataset of 1,700 synthetically generated coronary arteries to train and evaluate the model's performance. We split the data to train, validation and test set of sizes 1,500, 100 and 100, respectively.

We generate synthetic coronary arteries using ranges of geometric quantities such as the radii of branches, bifurcation angles, and degree of tapering with distributions similar to other studies [8,13]. On top of that, we model stenotic areas based on Coronary Artery Disease - Reporting and Data System (CAD-RADS) [16] stenoses percentage intervals. Our point clouds are further preprocessed such that each point is described by the position in the 3D space, Euclidean distance to the centerline and geodesic distance to the inlet (first point on the centerline).

For the ground-truth (GT) labels generation we use a commercial CFD engine of choice [10] designed for vFFR calculation.

The considered simulations for GT are stationary and take up to two hours on a CPU with 16 processes per synthetic coronary artery. We generate labels from a biologically relevant range that aim to simulate a patient under rest, mild exercise and high-intensity exercise conditions [12]. We experiment with three values of input flow Q_{in}: three, five and seven ml/s, and three values of inlet pressure p_{in}: 80, 100 and 120 mmHg.

Table 1. Comparison of PointNet++ (PN) and CenterlinePointNet++ (CPN) in the task of pressure drop and vFFR estimation with various BC of CFD GT simulation. Metrics are computed on the centerline-projected surface predictions.

	Q_{in}	Pressure drops						vFFR (p_{in} = 80 mmHg)			vFFR (p_{in} = 100 mmHg)			vFFR (p_{in} = 120 mmHg)		
	(ml/s)	NMAE (%)			MAE (m^2/s^2)			MAE ($\times 10^{-2}$)			MAE ($\times 10^{-2}$)			MAE ($\times 10^{-2}$)		
		mean	median	75th	mean	median	75th	mean	median	75th	mean	median	75th	mean	median	75th
PN	3	2.01	0.74	1.36	2.23	0.80	**1.52**	2.83	1.04	1.92	2.18	0.80	1.47	1.89	0.69	1.28
CPN		**1.57**	**0.55**	**1.32**	**1.75**	**0.64**	**1.52**	**2.21**	**0.77**	**1.86**	**1.70**	**0.60**	**1.43**	**1.47**	**0.52**	**1.24**
PN	5	1.68	0.63	1.31	4.31	1.59	3.35	5.36	2.01	4.17	4.13	1.55	3.21	3.58	1.34	2.78
CPN		**1.58**	**0.56**	**1.12**	**3.99**	**1.44**	**2.79**	**5.03**	**1.80**	**3.59**	**3.87**	**1.38**	**2.75**	**3.35**	**1.20**	**2.39**
PN	7	1.74	0.60	1.34	7.74	2.63	5.90	9.70	3.34	7.44	7.46	2.57	5.73	6.47	2.23	4.96
CPN		**1.54**	**0.50**	**1.17**	**6.86**	**2.23**	**5.18**	**8.56**	**2.80**	**6.50**	**6.58**	**2.16**	**5.00**	**5.71**	**1.87**	**4.33**

In our experimental setup, one coronary artery is composed of a surface point cloud with 100,000–200,000 points and a centerline graph with 300–600 vertices, depending on the complexity of the vascular tree. The surface point clouds are uniformly downsampled to 20,000 points during the training process. In the inference setting the per-point results are obtained via a mean aggregation over multiple inference runs, five in our case, of different random splits of a point cloud into chunks of 20,000 points. The process of projecting the surface features onto the centerline graph is done by averaging the estimated features of the faces' vertices which intersect with the orthogonal plane to the centerline placed for a given centerline node (Table 1).

3.2 Results

We showcase the comparison between PointNet++ and proposed CenterlinePointNet++ in the task of pressure drop and vFFR estimation for the synthetic dataset under different biologically relevant boundary conditions (BC) in Fig. 4. We report the MAE and NMAE which is MAE normalized by the absolute largest pressure drop in the testing set. The metrics are computed for projected results on a centerline for the evaluation to be more informative. CenterlinePointNet++ outperforms PointNet++ in every combination of input flow Q_{in} and inlet pressure p_{in} for both pressure drop and vFFR estimation.

We show a visual comparison between the PointNet++ and CenterlinePointNet++ capabilities in the task of the vFFR in Fig. 4 for two example synthetic simulations of a patient under rest with input flow Q_{in} of 3 ml/s and inlet pressure p_{in} of 80 mmHg. Both models tend to achieve good results on non-stenotic and mild-stenotic segments. However, when it comes to larger stenoses, PointNet++ lacks correct assessment of the stenosis impact, while CenterlinePointNet++ estimates correct values. We attribute this robustness towards sequential embedding done along the centerline which follows the natural blood flow in the coronary artery. Both examples in Fig. 4 showcase the common problem of PointNet++ for vessel trees with close branches. Since the aggregation is done via Euclidean distance, the branches close to each other in this space are considered neighbours. Due to that, the predicted vFFR on one branch tends to spill on

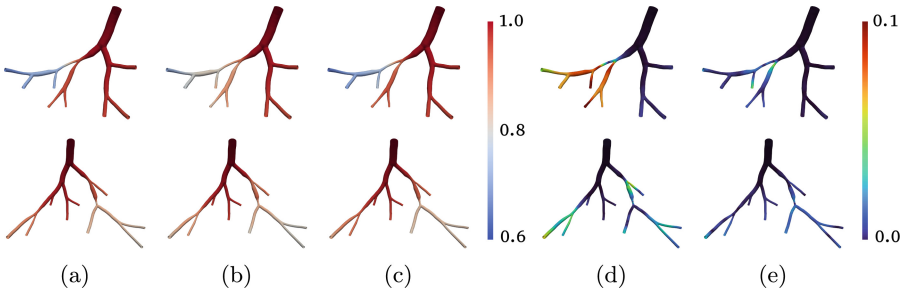

Fig. 4. Qualitative comparison of vFFR between PointNet++ and CenterlinePointNet++. (a) CFD GT vFFR, (b) PointNet++ vFFR, (c) CenterlinePointNet++ vFFR, (d) PointNet++ vFFR MAE, (e) CenterlinePointNet++ vFFR MAE on two examples. Due to the lack of sequential embedding, PointNet++ tends to be less robust in assessing the impact of stenosis on pressure drops.

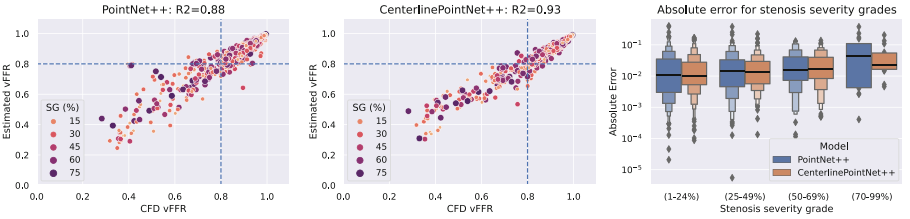

Fig. 5. Evaluation on vFFR estimation with respect to different stenosis severity grades. The vFFR is estimated at stenotic segments with the maximum percentage of radius change reported as a severity grade (SG). We report a correlation of 0.88 and 0.93 for PointNet++ and CenterlinePointNet++, respectively. Dashed lines at 0.8 indicate the clinical threshold.

the second branch as seen on the whole left side of the sample in the first row Fig. 4.

We evaluate estimated vFFR with respect to the stenosis severity grade and group stenosis grades into the relevant intervals based on CAD-RADS scale [16]. Figure 5 showcases scatter plots for PointNet++ vFFR and CenterlinePointNet++ vFFR estimation against GT CFD vFFR with respect to the stenosis severity grade. We report the correlation of 0.88 and 0.93 for PointNet++ and CenterlinePointNet++ vFFR estimation, respectively. Performance in correct stenosis impact assessment seems to deteriorate with the increase of stenosis severity grade, however, only outliers achieve the absolute error above 0.1. CenterlinePointNet++ vFFR estimations achieve smaller variations than PointNet++ over all classes, and significantly lower MAE for the stenosis severity grade (70–90%). We showcase that for the stenosis severity grade $\leq 70\%$ the median of CenterlinePointNet++ estimated vFFR absolute error is kept under 0.01. Additionally, we evaluate the clinical viability of the proposed method by computing the accuracy of whether to perform intervention or not based on

the predicted vFFR. We set the vFFR threshold to the clinically accepted one of 0.8 [2], and report the accuracy of 94.11% and 95.11% for PointNet++ and CenterlinePointNet++, respectively.

4 Conclusions

In this study, we propose a novel point cloud based neural network architecture CenterlinePointNet++ which is tailored towards the analysis of complex vessel trees by incorporating multi-modal input of surface point cloud and centerline graph. We show an improvement in the vFFR time estimation from approx. two hours for a CFD simulation to around 15 s per synthetic coronary artery. Our centerline grouping approach is confronted with PointNet++ in the task of pressure drop and vFFR estimation in synthetic coronary arteries and achieves better results in NMAE and MAE for every set of values of the input flow and pressure of CFD simulation. The evaluation of FFR showcases a correlation of 0.93 with the CFD vFFR. One of the limitations of the method is the fact that the model is trained for the specified set of boundary conditions of underlying CFD simulation. In the future, we plan to expand the approach by incorporating boundary conditions as an additional input to the network. We also aim to conduct a comprehensive study using real patients' geometries for both training and evaluation, while comparing the results with invasive FFR.

References

1. Arzani, A., Wang, J.X., Sacks, M.S., Shadden, S.C.: Machine learning for cardiovascular biomechanics modeling: challenges and beyond. Ann. Biomed. Eng. **50**(6), 615–627 (2022)
2. Corcoran, D., Hennigan, B., Berry, C.: Fractional flow reserve: a clinical perspective. Int. J. Cardiovasc. Imaging **33**, 961–974 (2017)
3. De Bruyne, B., Sarma, J.: Fractional flow reserve: a review. Heart **94**(7), 949–959 (2008)
4. Eldar, Y., Lindenbaum, M., Porat, M., Zeevi, Y.: The farthest point strategy for progressive image sampling. IEEE Trans. Image Process. **6**(9), 1305–1315 (1997). https://doi.org/10.1109/83.623193
5. de Haan, P., Weiler, M., Cohen, T., Welling, M.: Gauge equivariant mesh CNNs: anisotropic convolutions on geometric graphs. CoRR abs/2003.05425 (2020). https://arxiv.org/abs/2003.05425
6. Hamilton, W.L., Ying, R., Leskovec, J.: Inductive representation learning on large graphs. CoRR abs/1706.02216 (2017). https://arxiv.org/abs/1706.02216
7. He, J., et al.: Learning hybrid representations for automatic 3D vessel centerline extraction. In: Martel, A.L., et al. (eds.) Medical Image Computing and Computer Assisted Intervention – MICCAI 2020, pp. 24–34. Springer, Cham (2020). https://doi.org/10.1007/978-3-030-59725-2_3
8. Itu, L.M., et al.: A machine learning approach for computation of fractional flow reserve from coronary computed tomography. J. Appl. Physiol. (Bethesda, Md.: 1985) **121**, jap.00752.2015 (2016). https://doi.org/10.1152/japplphysiol.00752.2015

9. Ko, B.S., et al.: Noninvasive CT-derived FFR based on structural and fluid analysis: a comparison with invasive FFR for detection of functionally significant stenosis. JACC Cardiovasc. Imaging **10**(6), 663–673 (2017)
10. Kosior, A., Mirota, K., Tarnawski, W.: Patient-specific modeling of hemodynamic parameters in coronary arteries (20 June 2019), US Patent App. 16/217,328 (2019)
11. Li, G., et al.: Prediction of 3D cardiovascular hemodynamics before and after coronary artery bypass surgery via deep learning. Commun. Biol. **4**, 99 (2021). https://doi.org/10.1038/s42003-020-01638-1
12. Małota, Z., et al.: The comparative method based on coronary computed tomography angiography for assessing the hemodynamic significance of coronary artery stenosis. Cardiovasc. Eng. Technol. **14**, 364–379 (2023)
13. Medrano-Gracia, P., et al.: A study of coronary bifurcation shape in a normal population. J. Cardiovasc. Transl. Res. **10**(1), 82–90 (2017)
14. Morris, P.D., van de Vosse, F.N., Lawford, P.V., Hose, D.R., Gunn, J.P.: "virtual" (computed) fractional flow reserve: current challenges and limitations. JACC Cardiovasc. Interv. **8**(8), 1009–1017 (2015)
15. Nabel, E.G.: Cardiovascular disease. N. Engl. J. Med. **349**(1), 60–72 (2003)
16. Nikolaev, A., Feger, J., Weerakkody, Y., et al.: Coronary artery disease - reporting and data system. Reference article, Radiopaedia.org. https://doi.org/10.53347/rID-56786. Accessed 14 Feb. 2023
17. Qi, C.R., Su, H., Mo, K., Guibas, L.J.: PointNet: deep learning on point sets for 3D classification and segmentation. CoRR abs/1612.00593 (2016). https://arxiv.org/abs/1612.00593
18. Qi, C.R., Yi, L., Su, H., Guibas, L.J.: PointNet++: deep hierarchical feature learning on point sets in a metric space. CoRR abs/1706.02413 (2017). https://arxiv.org/abs/1706.02413
19. Rygiel, P., Zieba, M., Konopczynski, T.: Eigenvector grouping for point cloud vessel labeling. In: Bekkers, E., Wolterink, J.M., Aviles-Rivero, A. (eds.) Proceedings of the First International Workshop on Geometric Deep Learning in Medical Image Analysis. Proceedings of Machine Learning Research, vol. 194, pp. 72–84. PMLR, 18 November 2022. https://proceedings.mlr.press/v194/rygiel22a.html
20. Sklet, V.: Exploring the capabilities of machine learning (ML) for 1D blood flow: application to coronary flow. Master's thesis, Norwegian University of Science and Technology, Trondheim, Norway (2018)
21. Suk, J., Haan, P., Lippe, P., Brune, C., Wolterink, J.: Mesh convolutional neural networks for wall shear stress estimation in 3D artery models, September 2021
22. Taebi, A.: Deep learning for computational hemodynamics: a brief review of recent advances. Fluids **7**(6), 197 (2022). https://doi.org/10.3390/fluids7060197, https://www.mdpi.com/2311-5521/7/6/197
23. Verma, N., Boyer, E., Verbeek, J.: Dynamic filters in graph convolutional networks. CoRR abs/1706.05206 (2017). https://arxiv.org/abs/1706.05206
24. Wang, Z., et al.: Diagnostic accuracy of a deep learning approach to calculate FFR from coronary CT angiography. J. Geriatr. Cardiol. JGC **16**, 42–48 (2019)
25. Yao, L., et al.: TaG-Net: topology-aware graph network for vessel labeling. In: Manfredi, L., et al. (eds.) Imaging Systems for GI Endoscopy, and Graphs in Biomedical Image Analysis, pp. 108–117. Springer, Cham (2022). https://doi.org/10.1007/978-3-031-21083-9_11